Characterization of polybutadiene-poly(ethyleneoxide) aggregates in aqueous solution: A light-scattering and small-angle neutron-scattering study

Tobias Fuetterer, Anette Nordskog, Thomas Hellweg,* and Gerhard H. Findenegg
TU Berlin, Stranski-Laboratorium für Physikalische und Theoretische Chemie, Strasse des 17 Juni 112, D-10623 Berlin, Germany

Stephan Foerster
Universität Hamburg, Institut für Physikalische Chemie, Bundesstrasse 45, D-20146 Hamburg, Germany

Charles D. Dewhurst
Institut Laue-Langevin ILL, 6, rue Jules Horowitz, Boîte Postale 156, 38042 Grenoble Cedex 9, France
(Received 29 January 2004; published 28 October 2004)

For diblockcopolymers of polybutadiene-poly(ethyleneoxide) (PB-PEO) type, water is a selective solvent. In dependence of the length of both blocks and the block length ratio, these polymers form a multitude of self-assembled structures in solution. In the present work scattering methods are used to investigate the water-soluble polymer PB_{125}-PEO_{155}. It is found to form long rodlike micelles, which are characterized with respect to the aggregate length L, the cross sectional radius R_{CS}, the radial scattering length density profile $\sigma(r)$, and the radial aggregation number N_{rad}. Model-independent as well as model-based approaches are used for the scattering data analysis. From dynamic light scattering (DLS) and static light scattering (SLS) experiments the weight averaged length L_w of these stiff elongated aggregates is determined to $L_w = 350$ nm. Small angle neutron scattering (SANS) reveals a cross sectional radius of $R_{CS} = 17$ nm and in combination with results from the SLS the radial aggregation number is found to be $N_{rad} = 70$.

DOI: 10.1103/PhysRevE.70.041408 PACS number(s): 82.70.−y, 66.10.Cb, 61.12.Ex, 78.35.+c

I. INTRODUCTION

In recent years the self-assembly behavior of block copolymers (BCP's) in selective solvents was subject to an increasing number of studies [1–9]. The obtained size and shape of aggregates can be controlled by composition and molar mass of the two respective blocks. This leads to the potential use of BCP aggregates as templates for the synthesis of nanoporous materials or nanoparticles [10–15]. Various nanoporous geometries can be obtained using aggregates of different shape. Moreover, aqueous BCP solutions are of great interest because of their similarities with biological systems [16,17]. In several of these studies it was shown that light scattering is a useful technique to investigate the behavior of BCP's [7–9].

The phenomenon of self-assembly is already well known from surfactant systems. In contrast to surfactants, the dimensions of block copolymers are one order of magnitude larger and they have a very low critical micellar concentration (e.g., 3−5 mg/l for diblock oxyethylene/oxybuthylene copolymers [18], and see Refs. [19–23]). A BCP in solution can form cylindrical as well as spherical micelles at low concentrations [24,25]. The dominating structure of the BCP aggregates in a given system seems to depend on several different parameters, such as, for instance, the total length of the chain and the block length ratio of the hydrophilic and the hydrophobic part. These relations were investigated by Bates and co-workers [24] for the block copolymer poly(butadiene)-poly(ethyleneoxide) with different block length ratios using the method of Cryo-TEM. It was found that, at higher block volume ratio PEO to PB, spherical micelles are formed ($N_{PEO}/N_{total} > 0.6$), and at lower block volume ratios ($N_{PEO}/N_{total} \leqslant 0.6$) cylindrical micelles can be observed. For example PB_{104}-PEO_{166} forms cylindrical micelles in aqueous solution with a core diameter of around 16 nm and a total diameter of around 49 nm (from Cryo-TEM). In another work [26] Bates *et al.* investigated the core and shell dimensions of cylindrical and spherical aggregates in aqueous solutions by small angle neutron scattering (SANS). For PB_{69}-PEO_{132} ($N_{PEO}/N_{total} = 0.66$) they found spherical micelles with a core diameter of 22.4 nm and a total diameter of around 50 nm. The interfacial area per molecule is found to be $a_0 = 1.16\ nm^2$. For PB_{69}-PEO_{67}($N_{PEO}/N_{total} = 0.5$) they found cylindrical micelles with radial core diameter of 14.8 nm and a total radial diameter of 41.2 nm. The aggregation number per nm was determined as $N = 40\ nm^{-1}$ and the interfacial area per molecule is $a_0 = 1.18\ nm^2$. In a recent work by Won and co-workers [25] BCP of the type PEE-PEO were found to form not only spherical and wormlike micelles, but also vesicles in dependence on the block length ratio. They showed that there is a transition from bilayers (vesicles) via cylinders to spheres with increasing degree of polymerisation of the PEO block. It was also found that there is a broad overlapping range where two micellar structures coexist.

In addition to the variation of overall BCP length and block length ratio another approach to control the BCP-aggregate shape is known. By addition of low molecular weight amphiphils to BCP solutions it is possible to alter the packing parameter in the micellar structures.

*Author to whom correspondence should be addressed; Email address: thomas.hellweg@tu-berlin.de

In Ref. [27] Förster and co-workers investigated the different micellar structures of PB_{125}-PEO_{155} using mainly transmission electron microscopy (TEM) in a wide concentration range. The obtained micrographs revealed the existence of rodlike micelles in aqueous solutions of this BCP over the entire investigated concentration range from $c<0.02$ wt. % up to 30 wt. % [3,27,28]. However, due to the size of the aggregates it is a difficult task to obtain reliable averages for their length and their polydispersity from electron microscopy. Hence, in the present study we investigate the size, shape and polydispersities of PB_{125}-PEO_{155} micelles in dilute aqueous solution ($c=0.02$–2 wt. %) by means of static and dynamic light scattering. Application of these techniques to rod-like structures was reviewed by Russo [29]. Static light scattering (SLS) gives an experimental form factor $P(q)$ which can be fitted by the respective models. In addition the molar mass of the found aggregates is determined by SLS. The analysis of the dynamic light scattering (DLS) data is done with the model-independent inverse Laplace-transformation method and by applying a theory of Pecora developed to describe the dynamic behaviour of stiff rods [30,31]. In addition to the light scattering experiments also small angle neutron scattering (SANS) experiments are presented. SANS provides knowledge of the cross section of the PB_{125}-PEO_{155} aggregates.

II. MATERIALS AND METHODS

A. Polymer

The presented block-copolymer poly-butadiene-*b*-poly(ethylene-oxide) with the block lengths 125 and 155, respectively, was synthesized according to the procedure described by Förster *et al.* [28]. The analysis of the molecular weight of the polymer was performed by gel permeation chromatography (GPC) and the degree of polymerization of the PEO block was calculated from the molar ratios of PB/PEO from ^{1}H-NMR. The polydispersity, given by the ratio of M_w/M_n was found to be 1.02.

B. Light scattering (LS)

The solvent used for all light scattering experiments was high purity water from a Milli-Q water purification system by Millipore/Waters. A stock solution of 0.2 wt. % of polymer was diluted to 5 lower concentrations, namely, 0.16, 0.12, 0.08, 0.04, and 0.02 wt. %. All samples for the light scattering experiments were directly filtered into dust free cylindrical quartz cells (Hellma, Germany) with an inner diameter of 0.8 cm using filters with a pore size of 200 nm (Schleicher & Schuell, Spartan 30/0.2 RRC, or Whatman anotop 10).

LS measurements were performed using commercial equipment for simultaneous static and dynamic experiments from ALV-Laservertriebsgesellschaft (Langen, Germany). The light source employed was a Coherent 315M-150 frequency doubled diode pumped solid state laser, operating with a constant output power of 150 mW at $\lambda=532$ nm. Temperature control of the samples better than 0.1 K was achieved by using a Toluene thermostating bath, which also served as an index matching bath. The scattered light was detected with a photomultiplier tube (Thorn EMI) mounted on a goniometer arm, operated in single-photon-counting mode. The obtained preamplified fluctuating intensity signal was then time autocorrelated using an ALV-5000 multiple hardwire correlator (256 channels, first lag time 200 ns). Dynamic light scattering experiments were performed in an angular range between $30°<\theta<150°$, resulting in an agular range of $0.008<q<0.030$ nm^{-1}.

For the static light scattering experiments the static (integrated) intensity was normalized to the primary beam intensity and brought to absolute scale by using a toluene reference for calibration [32]. Consequently, the primary beam intensity had to be monitored, which was done by means of a beam splitter and a four-segment photodiode. Static LS measurements were carried out in an agular range of $20°<\theta<150°$, that corresponds to a scattering vector range of $0.008<q<0.030$ nm^{-1}. The refractive index increment dn/dc, which is necessary for the calculation of the contrast factor K, was measured with a commercial refractometer (DR1/b, Baur Electronics), $dn/dc=0.125$ g/g. The resulting contrast factor is $K=22.9$ mol cm^2 g^{-2} (see Sec. III A).

C. Small angle neutron scattering (SANS)

In SANS experiments diluted samples would exhibit a very low scattering intensity, which leads to unacceptable high measuring times. Therefore, compared to the light scattering experiments a higher concentration was used (2 wt. %). Scattering contrast for the small angle scattering experiments was generated by using D_2O from Sigma Fine Chemicals (isotopic purity >99.8%) as the solvent.

The small angle neutron scattering experiments presented here, were carried out at the Institute Laue-Langevin (ILL) in Grenoble, France, at the instrument D11. Making use of a mechanical selector (Dornier) the neutron wavelength was chosen to be 8 Å. The wavelength spread was approximately ±10%. The chosen sample-to-detector distances (1.1, 3, 5, 16, and 36 m) cover a q range from 0.0027 to 1.4 nm^{-1}. The data were collected on a two-dimensional ^{3}He detector with 64×64 elements. Due to the isotropic character of the scattering from the solutions under investigation, the raw data were circularly averaged. After correction for the scattering of the solvent and the empty cell, the data were brought to absolute scale. Calibration of the data was done with H_2O as the standard. All the data reduction steps described above were done using the software package GRASP provided by the ILL.

III. THEORY

A. Static light scattering (SLS)

The normalized static light scattering intensity $R(q)$ (Rayleigh-Ratio) for particles in dilute solution can be written as [32]

$$R(q) = KcM_wP(q)S(q), \tag{1}$$

where c is the mass concentration, $P(q)$ is the particle form factor, $S(q)$ is the structure factor, and q is the magnitude of the wave vector

$$q = 4\pi \frac{n}{\lambda_0} \sin\left(\frac{\theta}{2}\right), \tag{2}$$

with the scattering angle θ and K is the contrast factor given by

$$K = 4\pi^2 \frac{n^2}{\lambda_0^4} N_A \left(\frac{dn}{dc}\right)^2, \tag{3}$$

with the refractive index n of the solution, the wavelength λ_0 of the radiation, the Avogadro constant N_A, and the refractive index increment dn/dc of the particles. In the highly diluted regime the structure factor $S(q)=1$ and can be neglected. Then the q dependence of $R(q)$ is described by the particle form factor $P(q)$. A common representation of Eq. (1) to analyse SLS data with respect to the weight-average molar mass M_w and the z average of the radius of gyration $R_{g,z}$ is [33–35]

$$\frac{Kc}{R(q)} = \frac{1}{M_w}\left(1 + \frac{1}{3}R_{g,z}^2 q^2\right), \tag{4}$$

where the form factor $P(q)$ is replaced by its Debye approximation. For elongated structures, as wormlike micelles, several model form factors can be used to analyze the measured q dependence of $R(q)$. As the cross section of micellar wormlike structures do not affect $R(q)$ in the q regime of the light scattering experiments, the different models only have to consider different degrees of stiffness and a distribution of the contour length L of the wormlike aggregates. The most simple approach for a data analysis is a model form factor $P(q)_{\mathrm{rod}}$ for stiff thin cylinders with monodisperse length L [36]

$$P(q)_{\mathrm{rod}} = \frac{2}{qL}\int_0^{qL} \frac{\sin(ql)}{ql} dql - 4\left(\frac{\sin(qL/2)}{qL}\right)^2. \tag{5}$$

For self-assembled wormlike aggregates it is obvious to consider a length distribution. For several investigated equivalent systems [37–40] an asymmetric distribution $p(k,L,L_w)$ according to Schulz-Zimm [41] is used to describe such a length distribution

$$p(k,L,L_w) = \frac{[(k+1)/L_w]^{k+1} L^k \exp[-(k+1)L/L_w]}{\Gamma(k+1)}, \tag{6}$$

with $k=1/(M_w/M_n-1)$, the gamma function $\Gamma(k+1)$, and the mass average of the contour length L_w. Taking into account this length distribution as the measured z average of the contour length L the form factor for stiff rods [Eq. (5)] then becomes [37]

$$P(q)_{\mathrm{poly}} = \frac{\int_0^\infty L\, p(k,L,L_w)\, P(q) dL}{\int_0^\infty L\, p(k,L,L_w) dL}. \tag{7}$$

The number average L_n, the mass average L_w, and the z average L_z of the contour length L are given by

$$L_n = \frac{\sum_i N_i L_i}{\sum_i N_i}, \quad L_w = \frac{\sum_i N_i L_i^2}{\sum_i N_i L_i}, \quad L_z = \frac{\sum_i N_i L_i^3}{\sum_i N_i L_i^2}, \tag{8}$$

with the number N_i of aggregates with length L_i. The flexibility of wormlike aggregates can be described in terms of the ratio between the contour length L_w and the Kuhn-length L_K. For the q range of light scattering experiments Koyama [42] has derived a form factor $P(q)_{\mathrm{WC}}$ for flexible wormlike chains

$$P(q)_{\mathrm{WC}} = \frac{1}{l_K^2}\int_0^{l_K} (l_K - x)\exp\left(-\frac{1}{3}(q')^2\, xf(x)\right)\frac{\sin[q'\, xg(x)]}{q'\, xg(x)} dx, \tag{9}$$

with the dimensionless quantity l_K defined by Koyama, which is related to the contour length L. The functions $q', xf(x), xg(x)$ are defined in Koyama's publication [42], where $xf(x)$ and $xg(x)$ are functions of the Kuhn length L_K. The Kuhn length L_K is the length of a stiff segment in the flexible aggregate chain. As can be seen from Eq. (9) this form factor includes the form factor for stiff rods with length L_K at high-q values and a Guinier approximation to account for the large scale structure of the particles at low-q values. As in the case of the model for stiff rods a length distribution can be considered here [see Eq. (7)]. Applying Eq. (7) to the static light scattering data will lead to information about the average contour length L_w, the polydispersity parameter k, and the flexibility L_w/L_K of the aggregates. It should be mentioned here that the Koyama approach is only valid when the flexibility of the investigated aggregates is low (which is the present case). For structures with a significantly higher flexibilty better description were given by Pedersen and coworkers [43,44].

If the cylindrical aggregates are stiff, the q dependence should be describable with the form factor for stiff rods but if the aggregates are markedly flexible significant deviations between the model form factor $P(q)_{\mathrm{rod,poly}}$ and the data should occur. The form factor of Koyama, $P(q)_{\mathrm{WC,poly}}$, should be valid for both, stiff and flexible aggregates. A ratio $L_w/L_K=1$ is characteristic for stiff and $L_w/L_K \gg 1$ is characteristic for flexible aggregates.

B. Small angle neutron scattering (SANS)

The analysis of the SANS data is based on the same principles as outlined for the static light scattering data. Small-angle scattering curves from colloidal solutions can be represented by

$$I(q) = C\Delta\sigma^2 P(q) S(q), \tag{10}$$

where C is a concentration-dependent factor, and $\Delta\sigma$ is the excess scattering length density of the particles ($\Delta\sigma = \sigma_{\mathrm{particle}} - \sigma_{\mathrm{solvent}}$). For low concentrations and intermediate or large values of q for spherical [45,46] and also for rodlike particles $S(q)=1$ [47], hence the analysis of the experiments has mainly to focus on the particle form factor. The structure factor of rodlike particles in concentrated solutions was dis-

cussed by Weber *et al.* [48] and by Klein *et al.* [49]. However, in the present study the concentration is sufficiently low and hence, only the form factor will be considered in the following.

Due to the q range in a SANS experiment the dimension of the cross sectional radius R_{CS} of the rods has to be taken into account in the form factor. For cylinders with a given cross-sectional radius, Eq. (5) transforms into [36]

$$P(q)_{cyl} = \int_0^{\pi/2} \left(2\frac{J_1(qR_{CS,hom}\sin(\alpha))}{qR_{CS,hom}\sin(\alpha)} \cdot \frac{\sin\left(\frac{1}{2}qL\cos(\alpha)\right)}{\frac{1}{2}qL\cos(\alpha)} \right)^2 \times \sin(\alpha) d\alpha. \quad (11)$$

J_1 is the spherical Bessel function of the first order and $R_{CS,hom}$ is the cross-sectional radius assuming a homogeneous scattering length density over the cross section. The angle α is enclosed by the scattering vector q and the long axis of the cylinder. A Schulz-Zimm distribution of the length L can be considered as in the case of the form-factor of a stiff rod [see Eq. (7)].

A model-independent analysis of the SANS data according to the indirect Fourier transformation method by Glatter [50–52] yields the pair distance distribution function $p(r)$, and the Fourier transform of $p(r)$ represents $I(q)_{fit}$,

$$I(q)_{fit} \propto 4\pi \int_0^{\infty} p(r)\frac{\sin(qr)}{qr} dr. \quad (12)$$

If the data analysis is made for a broad q-range the pair distance distribution function $p(r)$ is affected by the length of the cylinders. For different three-dimensional particle shapes the one-dimensional $p(r)$ function shows characteristic features and allows to differentiate between different particle shapes [50]. If only the high-q range is enclosed in the analysis and the particle symmetry (cylinder) is predefined the $p(r)$ function of the cross section is computed and thus an upper limit for the cross sectional radius. With the assumption that the cross section is radially symmetric the deconvolution of $p(r)$ gives the radial scattering length density distribution function $\sigma(r)$ [53]. The software package ITP by Glatter [50–52] is used for this data analysis. From the cross sectional $p(r)$ function an equivalent radius of a homogeneous cross section $R_{CS,equi}$ can be calculated and compared to the radius $R_{CS,hom}$ from the form-factor analysis. The square of $R_{CS,equi}$ is given by [53]

$$R_{CS,equi}^2 = \frac{\int_0^{\infty} p(r) r^2 dr}{\int_0^{\infty} p(r) dr}. \quad (13)$$

C. Dynamic light scattering (DLS)

The scattering intensity I at a given scattering vector $\vec{q}$ depends on the relative positions of the scattering particles in the scattering volume. The diffusion of the particles results in an intensity fluctuation $I(t)$, with t representing time. I is proportional to the square of the scattered electric field $\langle E \rangle^2$. The fluctuations of I or E can be analyzed in terms of correlation functions [54]. The normalized electric field autocorrelation function $g_1(\tau)$ contains the information about the dynamics of the scatterers. In polydisperse samples each particle size contributes to $g_1(\tau)$ with a specific exponential decay. Hence the correlation function is given by a weighted sum of exponentials

$$g_1(\tau) = \int_0^{\infty} G(\Gamma)\exp(-\Gamma\tau) d\Gamma, \quad (14)$$

where $G(\Gamma)$ is the distribution function of relaxation rates $\Gamma, \Gamma = D_{tr}q^2$, with D_{tr} the translational diffusion coefficient [30]. $g_1(\tau)$ can be measured directly in a heterodyne light scattering experiment. However, it is more convenient to perform a homodyne experiment, which leads to the intensity time autocorrelation function $g_2(\tau)$,

$$g_2(\tau) = \frac{\langle E^*(t)E(t)E^*(t+\tau)E(t+\tau)\rangle}{\langle I \rangle^2}. \quad (15)$$

$g_1(\tau)$ and $g_2(\tau)$ are connected by the Siegert relation

$$g_2(\tau) = a|g_1(\tau)|^2 + b, \quad (16)$$

where a is the amplitude and b a baseline parameter. These two parameters have the value one in a perfect experiment. The data for $g_1(\tau)$ can be analyzed in a model-independent way. Most common is the analysis by an inverse Laplace transformation of $g_1(\tau)$, using the FORTRAN program CONTIN [55,56]. The resulting relaxation rate distribution function $G(\Gamma)$ contains information about the z-averaged relaxation rate $\overline{\Gamma}$, and the polydispersity. In the present system the particles have a highly anisotropic shape, which leads to contributions from translational as well as rotational diffusion. Several models have been proposed to describe the dynamic behavior of cylindrical or wormlike particles. The cylindrical particles presented in this work are stiff, i.e., the Kuhn-length L_K is of similar magnitude as the contour length L. To describe these stiff elongated particles we use a model of stiff rods derived by Pecora [29,31,54], which accounts for the rotational and the translational motions. The translational motion can be described by one averaged diffusion coefficient D_{tr} which is independent of the rotational diffusion (D_{rot}). The overall motion of the particle is determined by combinations of translation and rotation. As can be seen from Eq. (17), the resulting intermediate scattering function is a sum of these different types of motion. The amplitudes S_n of the resulting modes relate to different length scales in relation to the length L, as they depend on the product of q and the length L.

$$g_{1,\mathrm{rod}}(\tau,L) = \sum_{n=0}^{3} S_n(2n,qL) \times \exp(-\{D_{\mathrm{tr}}q^2 + [2n(2n+1)] \cdot D_{\mathrm{rot}}\} \cdot \tau). \quad (17)$$

The amplitudes S_n are proportional to the square of the integral over a spherical Bessel function of 2nd order [29]. For values of $qL \leqslant 4$, only the pure translation (S_0) contributes to the intermediate scattering function. For values of $qL \leqslant 15$, the first three modes have to be taken into account [29]. In the present study qL has a maximum value of around 15 ($q_{\max} = 0.03\ \mathrm{nm}^{-1}$ and $L_{\max} = 500$). In most of the previous publications using this model only the modes with $n=0$ and $n=1$ are taken into account. Both the translational diffusion coefficient and the rotational diffusion coefficient depend on the geometry (length L, diameter d) and flexibility (L_w/L_K) of the rods. For rigid particles, Kirkwood and Riseman derived a relation between the diffusion coefficients and the particle geometry, based on the Oseen approximation [57], viz.,

$$D_{\mathrm{tr}} = \frac{k_B T}{3\pi\eta_0 L}\ln\left(\frac{L}{d}\right) \text{ and } D_{\mathrm{rot}} = \frac{9D_{\mathrm{tr}}}{L^2}, \quad (18)$$

where k_B is the Boltzmann constant, T the temperature, and η_0 the viscosity of the solvent. The model of Broersma [58,59], even in its corrected form, does not provide a better representation than the simple Kirkwood-Riseman approach [29]. However, for real systems the distribution of rod lengths L has to be taken into account. In the present work, the Schulz-Zimm distribution was adopted. The measured $g_2(\tau)$ of polydisperse stiff rods can be analyzed by applying Eq. (17) in combination with the Siegert relation [Eq. (16)]. This model-based analysis leads to the average length L_w, the diameter d, and the shape and width of the length distribution. The field correlation function $g_1(\tau)$ is then given by

$$g_{1,\mathrm{rod}}(\tau) = \frac{\sum_L Lp(k,L,L_w)g_{1,\mathrm{rod}}(\tau,L)}{\sum_L Lp(k,L,L_w)}, \quad (19)$$

where $p(k,L,L_w)$ is the mass distribution [Schulz-Zimm, Eq. (6)] of length L. The diffusion coefficients D_{tr} and D_{rot} were calculated from the length L and the diameter d using the Kirkwood-Riseman relation (18). The parameters of the model are independent of q, except the amplitude a. Hence a parameter set for a given q value must describe the dynamic behavior at other q values as well. To implement this into the data analysis, a simultaneous fit of $g_2(\tau)$ at four different q values was performed, where only the amplitudes a can have different values for the different q values. The length L_w and the polydispersity parameter k have the same values for the four different angles. The baseline parameter b is set to the individual constant value at high correlation times of $g_2(\tau)$ at the different q values ($b_{\mathrm{exp}} = 1 \pm 0.004$ covers all cases).

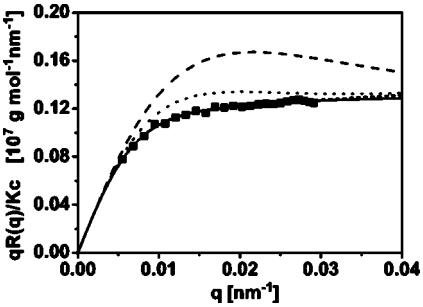

FIG. 1. Holtzer-plot of the experimental Raleigh-Ratio $R(q)/Kc = M_w P(q)$ of a 0.02 wt. % PB_{125}-PEO_{155} solution in H_2O at 25 °C (symbols). Model form factors are fitted to the data: polydisperse rod (straight line) with $L_w = 389$ nm and $M_w/M_n = 1.2$; polydisperse wormlike chain with $L_w = 380$ nm, $M_w/M_n = 2$, and $L_K = 410$ nm (---). As a comparison the model form factors of wormlike chains with a higher flexibility, i.e., lower Kuhn-length L_K, are depicted, too $L_K = 200$ nm ($\cdots$) and $L_K = 100$ nm (---).

IV. RESULTS AND DISCUSSION

A. Static light scattering (SLS)

SLS was performed with a 0.02 wt. % solution of PB_{125}-PEO_{155} in water. Analyzing the initial slope of $Kc/R(q)$ vs q^2 at low-q values gives the z average of the radius of gyration $R_g = 124$ nm according to Eq. (4). The intercept gives the molar mass $M_w = 1.62 \times 10^8$ g/mol. To analyze the whole experimental q range this low-concentration curve is plotted as a Holtzer diagram [$qR(q)/Kc$ vs q] in Fig. 1. In the same figure also the form factors used for the analysis are shown: polydisperse rigid rod [Eqs. (5) and (7)] and polydisperse wormlike chain [Eqs. (7) and (9)]. As one can see, both the form factor for polydisperse rigid rods and wormlike chains describe the experimental data similarly well, although the form factor for polydisperse rigid rods has no flexibility included and the form factor for wormlike chains of Koyama is for flexible aggregates. The mass-averaged lengths L_w of the aggregates were found to be 389 and 380 nm, respectively (see Table I). The Kuhn length given from the Koyama fit is 410 ± 30 nm (from $L_K = 380$ to 440 the quality of the fit is $\chi^2 \leqslant 1.1\chi^2_{\min}$). This values equal the contour length, and hence one can say that the aggregates must have a very low degree of flexibility and that they are approximately stiff. As a comparison in Fig. 1 the form-factor for wormlike aggregates (Koyama) is plotted for different decreasing values of the Kuhn length L_K, i.e., for a higher flexibility. These form factors for wormlike chains with a non-negligible degree of flexibility are not able to describe the measured q dependence. Both applied form factors account for polydispersity using a Schulz-Zimm distribution. The polydispersity in terms of M_w/M_n resulting from the form-factor fits is also given in Table I. The respective experimental values of around 1.5 are in good agreement with other experimental results for such self-assembled wormlike chains [37–39]. From the distribution function [Eq. (6)] the number and z average of the contour length can be calculated according to Eq. (8) (see Table I).

To make sure that the values for $L_w, M_w/M_n$, and L_K derived from the fits are physically meaningful, it was checked

TABLE I. Structural parameters for PB_{125}-PEO_{155} aggregates in aqueous solution (0.02 wt. % $< c <$ 2 wt. %) as obtained by analyzing the SLS, DLS, and SANS data.

	SLS			DLS		SANS	
	Eq. (4)	Koyama	Rod	CONTIN	Pecora(Rod)	IFT	Cylinder
$R_{g,z}$(nm)	124						
$R_{H,z}$(nm)				60 ± 6	81		
$R_{g,z}/R_{H,z}$		2[a]	1.6[b]	2	1.8		
$D_{\mathrm{tr},z}(\mathrm{m}^2/\mathrm{s})$				$4\pm0.4\times10^{-12}$	3.02×10^{-12}[c]		
M_w/M_n		2.0	1.2		1.5–2		1.3
L_n(nm)		254	325		190 ± 50		191
L_w(nm)		380	389		340 ± 30	200[d]	250
L_z(nm)		508	455	290	475 ± 40		305
L_K(nm)		410 ± 30					
$R_{g,z}$(theor)		122[e]	130[f]		146[f]		97
M_w(g/mol)	1.62×10^8	1.67×10^8	1.68×10^8				
$M_w/L_w(\mathrm{g/mol_{nm}})$		4.4×10^5	4.3×10^5		4.9×10^5		
R_{CS}(nm)						19[d]	14
$R_{H,\mathrm{CS}}$(nm)					13–15		

[a]With $R_{H,z}$ from CONTIN and $R_{g,z}$(theor.).
[b]With $R_{H,z}$ from Pecora-model and $R_{g,z}$(theor.).
[c]With Eq. (18) using $d=28$ nm and $L_z=475$ nm.
[d]Maximum dimension from $p(r)$.
[e]With Eq. (20).
[f]With Eq. (21).

that they reproduce the experimental value of the radius of gyration $R_{g,z}$ determined according to Eq. (4), as given by the formula of Benoît and Doty [38,41] for polydisperse wormlike chains

$$R_{g,z}^2 = L_k\frac{k+2}{6y} - \frac{L_k^2}{4} + \frac{L_k^3}{4L_w} - \frac{L_k^4}{8k(k+1)}\left(y^2 - \frac{y^{k+2}}{y+2/L_k}\right), \tag{20}$$

with $y=(k+1)/L_w, k=1/(M_w/M_n-1)$ and L_w is the weight-average of the contour length. For rigid rods $R_{g,z}$ is given by [41]

$$R_{g,z}^2 = \frac{(k+3)(k+2)}{(k+1)^2}\frac{L_w^2}{12}. \tag{21}$$

For both form factors the experimental radius of gyration $R_{g,z}=124$ nm is reproduced with good accuracy, $R_{g,z}=122$ nm and $R_{g,z}=130$ nm, respectively (see Table I). From the fits of $R(q)/Kc$ with the model form factors the aggregates molar mass is obtained from the intercept [see Eq. (1)]. The acquired values are $M_w=1.67\times10^8$ g/mol for the model of Koyama and $M_w=1.68\times10^8$ g/mol for the model of polydisperse rods. These values are approximately independent of the concentration c, since the solution under investigation is highly diluted ($c=0.02$ wt.%) and the dynamic light scattering experiments (see below) only reveal a minor concentration dependence of the translational diffusion coefficient $D_{z,\mathrm{app}}$ (see Fig. 7). This clearly indicates that $S(q)=1$ at a concentration of 0.02 wt. %. The molar mass and the mass averaged contour length L_w give the linear mass density of the aggregates $M_L=M_w/L_w=4.7\times10^5$ g mol^{-1} nm^{-1} (with $L_w=370$ nm and $M_w=1.65\times10^8$ g/mol, see Table I). From the molar mass $M_{w,p}=13\,570$ g mol^{-1} of a single polymer molecule the aggregation number N_{M_w} and from the linear mass density M_L the aggregation number per nm $N_{M_w,\mathrm{nm}}$ of the aggregates can be estimated by $N_{M_w}=M_w/M_{w,p}=12\,100$ and $N_{M_w,\mathrm{nm}}=M_L/M_{M_w,p}=35$ nm^{-1}.

For comparison these two aggregation numbers can also be calculated from the aggregate volume $V_a=\pi R_{\mathrm{CS}}^2 L_w = 2.15\times10^5/4.0\times10^5$ nm^3 (see Table I) and an estimated volume of a single polymer molecule $V_{\mathrm{BCP}}=35.3$ nm^3 (according to Ref. [60] and see Refs. [61,62], per EO segment two H_2O molecules are taken into account). The aggregation number is than given by $N_V=V_a/V_{\mathrm{BCP}}=11\,240$ and the aggregation number per nm is given by $N_{V,\mathrm{nm}}=V_a/(L_w V_{\mathrm{BCP}}) = 32$ nm^{-1}. To calculate the radial aggregation number N_{rad} the length of one PB_{125}-PEO_{155} molecule along the aggregates long axis $l_{\mathrm{BCP,cyl}}$ must be estimated, $N_{\mathrm{rad}} = N_{V,\mathrm{nm}} l_{\mathrm{BCP,cyl}}$. The area A_{BCP} of one BCP molecule at the cylinder surface can be calculated by $A_{\mathrm{BCP}}=A_{\mathrm{cylinder}}/N_V = 5$ nm^2, with $A_{\mathrm{cylinder}}=2\pi R_{\mathrm{CS}} L_w=30.8\times10^3$ nm^2. Assuming a squared surface area per BCP molecule the surface length $l_{\mathrm{BCP,cyl}}$ is $\sqrt{A_{\mathrm{BCP}}}=2.2$ nm. The resulting radial aggregation number is $N_{\mathrm{rad}}=70$. The headgroup area a_0 of a PB_{125}-PEO_{155} molecule in the aggregate is given by $a_0 = A_{\mathrm{core}}/N_V=2.29$ nm^2, with $A_{\mathrm{core}}=2\pi R_{\mathrm{core}} L_w=25\,730$ nm^2. R_{core} can be estimated from the volume V_{BCP}, the volume of the PB block, $V_{\mathrm{PB}}=13.5$ nm^3, and the radius $R_{\mathrm{CS}}=19$ nm and is calculated to $R_{\mathrm{core}}=11.7$ nm. From the headgroup area a_0, the volume of the hydrophobic segment V_{PB} and the length

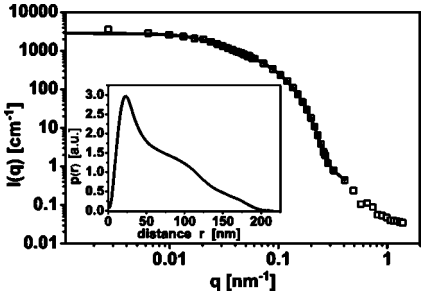

FIG. 2. SANS intensity of 2 wt. % PB_{125}-PEO_{155} in D_2O at 25 °C (symbols). The line represents the Fourier transform of the pair distance distribution function $p(r)$. Inset: Pair distance distribution function $p(r)$ obtained by indirect Fourier transformation of the measured data.

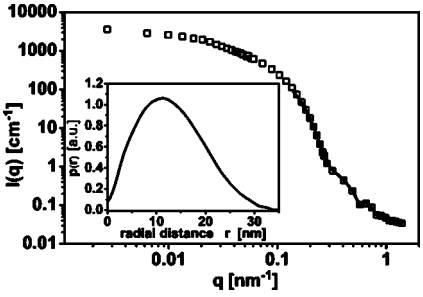

FIG. 3. SANS intensity of 2 wt. % PB_{125}-PEO_{155} in D_2O at 25 °C (symbols). The line represents the Fourier transform of the radial pair distance distribution function $p(r)$. Inset: Radial pair distance distribution function $p(r)$ obtained by inverse Fourier transformation of the measured data (high-q range). During the transformations the cylindrical shape is predefined to obtain the two-dimensional radial pair distance distribution function of the cross section.

of the hydrophobic segment R_{core} the packing parameter P can be calculated according to

$$P = \frac{V_{\mathrm{PB}}}{a_0 R_{\mathrm{core}}}. \tag{22}$$

The resulting value is $P=0.50$. In the range $0.333<P<0.5$ cylindrical particles are expected and from 0.5 to 1 flexible double layers are expected. The found value of $P=0.5$ is consistent with the cylindrical shape already assumed by using the from factors of a cylinder and a wormlike chain. One can conclude that a model for stiff rods with a Schulz-Zimm length distribution describes most of the features of the block-copolymer aggregates under investigation, and hence, justifies the use of the Pecora-model for rigid rods with a Schulz-Zimm-like polydispersity to describe the DLS data.

B. Small angle neutron scattering (SANS)

SANS is used to determine the cross sectional radius R_{CS}, and the radial scattering length density profile $\sigma(r)$ of the cylindrical aggregates.

1. Model-independent analysis

In Fig. 2 the experimental SANS intensity $I(q)$ of a 2 wt. % PB_{125}-PEO_{155} solution in D_2O is depicted. The analysis of a broad experimental q range including the low-q values with the IFT method gives the pair distance distribution function $p(r)$ shown in the inset in Fig. 2. In the analyzed q range, $0.0027\ \mathrm{nm}^{-1}<q<0.4\ \mathrm{nm}^{-1}$, aggregate dimensions from 12 to 500 nm determine the q dependence of $I(q)$. The upper limit is a measure for the aggregate length L and the lower limit equals approximately the cross sectional radius R_{CS}. The resulting shape of the two-dimensional $p(r)$ function is typical for cylindrical particles. The maximum length scale ($r_{\mathrm{max}}\approx 200$ nm) is significantly below the aggregate length L_w determined with SLS (see above) and DLS (see below). This might be due to an influence of the structure factor $S(q)$ at low-q values. A discussion of this effect is given below (model-dependant analysis).

The software ITP by Glatter gives the possibility to predefine a particle shape during the analysis. In case of a cylinder this reduces the analysis of a three-dimensional anisotropic shape to the analysis of a two-dimensional radial symmetric geometry, the cross section of the cylinders. The deconvolution of the resulting radial pair-distance distribution function $p(r)$ is the radial excess scattering length density profile $\sigma(r)$ [53]. In Fig. 3 the experimental SANS intensity $I(q)$ of a 2 wt. % PB_{125}-PEO_{155} solution in D_2O is depicted again. Analyzing the high q range of $I(q)$ ($0.1\ \mathrm{nm}^{-1}<q<1.4\ \mathrm{nm}^{-1}$) with the IFT method and a predefined cylindrical shape gives a maximum dimension of the cross section $d_{\mathrm{CS,max}}=35$ nm. From the resulting radial pair distance distribution function $p(r)$ (see inset in Fig. 3) the radial excess scattering length density profile $\sigma(r)$ is calculated. The resulting profile is plotted in Fig. 4 and it is consistent with a core shell cylinder model, when the alkyl chains (PB) are forming the core and the hydrophilic oxyethylene chains (PEO) are forming the outer layer (corona): In this case, the core will exhibit the highest contrast against the solvent (D_2O), while the hydrated oxyethylene chains will exhibit a much smaller contrast. The shape is similar to chemically comparable self assembled wormlike aggregates [39,63] and the upper limit of the cross sectional radius can be estimated to $R_{\mathrm{CS,dis}}=19$ nm.

2. Model-dependent analysis

In Fig. 5 the experimental SANS intensity $I(q)$ of a 2 wt. % PB_{125}-PEO_{155} solution in D_2O is depicted again. The q

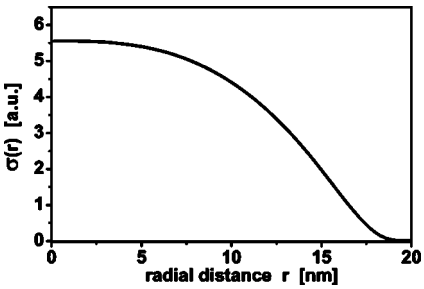

FIG. 4. Radial excess scattering length density distribution function obtained by deconvolution of $p(r)$ (see Fig. 3) for the cylinder aggregates.

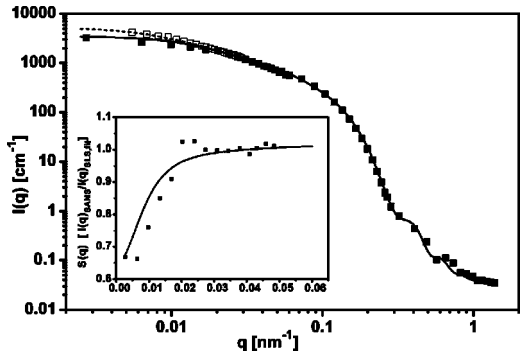

FIG. 5. SANS curve $I(q)_{\mathrm{SANS,expt}}$ of a 2 wt. % PB_{125}-PEO_{155} solution in D_2O at 25 °C (full symbols). The solid line is a simulation according to a form factor of a cylinder (L_w = 250 nm, $R_{\mathrm{CS,hom}}$ = 14 nm) with a Schulz-Zimm length distribution, but monodisperse cross section, including smearing effects. In the q range from 0.003 to 0.06 nm^{-1} a wavelength distribution of the neutron beam of 10% is considered and for the high-q range (0.06 to 1.5 nm^{-1}) a wavelength spread of 20% is used in the simulation. The open symbols indicate the SLS intensity (see Fig. 1) and the dotted line is the fit of a form factor of a rod, $I(q)_{\mathrm{SLS,fit}}$. Inset: ratio between the SANS intensity $I(q)_{\mathrm{SANS,expt}}$ (symbols) and $I(q)_{\mathrm{SANS,fit}}$ (line) to the fitted SLS intensity $I(q)_{\mathrm{SLS,fit}}$.

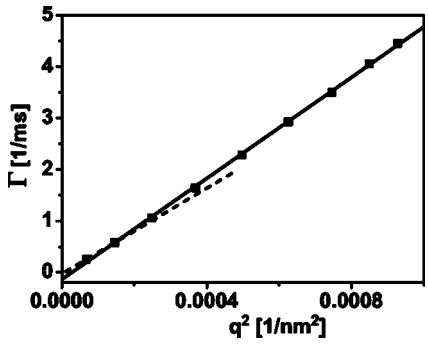

FIG. 6. Average relaxation rates Γ as a function of q^2 obtained by a CONTIN analysis of $g_1(\tau)$ from a 0.2 wt. % solution of PB_{125}-PEO_{155}. The straight line is a linear fit over all values of Γ resulting in $\langle D_{\mathrm{z,app}} \rangle$ and the dashed line is a regression over the two Γ values at low-q resulting in $D_{\mathrm{z,app}}$.

dependence of $I(q)$ can be well described over the whole q range using a model form factor for stiff cylinders with a Schulz-Zimm distribution of the length L. This form factor does not account for a size distribution of the cross sectional radius. But a size distribution of the cross sectional radius is considered in terms of the wavelength distribution of the neutron beam. In both cases, a Gaussian size distribution of a radius or a Gaussian wavelength distribution of the scattered radiation, the effects on $I(q)$ are identical. For the simulation of a smeared form factor of a cylinder with a polydisperse cross-sectional radius, a wavelength distribution of 20% was used for the intermediate and high q region of the measured SANS data (0.06 nm$^{-1} < q <$ 1.4 nm^{-1}). This value of 20% is twice the given spread of 10% for the used SANS machine. As the wavelength distribution is of Gaussian type, the overestimated value of 20% accounts for a Gaussian distribution of the cross sectional radius with a spread of $\sqrt{0.2^2 - 0.1^2} = 0.17$. For the low-$q$ region of the measured SANS data (0.0027 nm$^{-1} < q <$ 0.06 nm^{-1}) the given value of 10% for the wavelength distribution is used. In the low-q region only the length of the aggregates affect $P(q)$ and for the length L the Schulz-Zimm distribution is already included in the form factor. Smearing effects on the data due to the experimental conditions (collimation length, detector-pixel smearing, aperture, detector-sample distance, wavelength, and wavelength distribution) are considered according to Ref. [64]. The minor deviations between the smeared form factor and the measured data for high-q values might be due to the homogeneous cross sectional scattering length density assumed in the model compared to the cross sectional scattering length density profile of a real particle. The resulting cross sectional radius is $R_{\mathrm{CS,hom}}$ = 14 nm. The found mass average length L_w = 250 nm is somewhat lower compared to the results of the static light scattering analysis. This might be due to the non-negligible influence of $S(q)$ at low-q values. Due to the low scattering intensity compared to light scattering SANS is performed on a 2 wt. % solution of PB_{125}-PEO_{155} in D_2O, which is a 10–100 times higher concentration as for the light scattering experiments. Whereas for the high-q range the structure factor $S(q)$ can still be neglected, an influence of $S(q)$ on $I(q)$ in the low-q range is observable. $S(q)$ decreases the scattering intensity at low q, resulting in an underestimation of the particle length. For comparison the static light scattering data (see above) are depicted in Fig. 5, too. The SLS data are scaled by a constant factor to align them to the SANS data. At low-q values a significant deviation is observed resulting in the different values of L_w for the two methods or rather the two concentrations. The deviation can be analyzed in terms of the ratio between $I(q)_{\mathrm{SANS}}$ and $I(q)_{\mathrm{SLS}}$. $I(q)_{\mathrm{SLS}}$ is represented well by the fitted model curve. Therefore, the ratio is calculated from this model curve $I(q)_{\mathrm{SLS,fit}}$ and first from the measured SANS data (symbols in the inset of Fig. 5) and second from the model curve fitted to the SANS data (line in the inset of Fig. 5). The shape of the resulting curves can be attributed to a structure factor effect (e.g., Ref. [65]).

The cross sectional radius $R_{\mathrm{CS,hom}}$ from the form-factor analysis and the results on R_{CS} from the indirect Fourier transformation method (IFT) can be compared. According to Eq. (13) the radial pair distance distribution function $p(r)$ (see Fig. 3) can be transformed into a respective $R_{\mathrm{CS,equi}}$. The resulting value of $R_{\mathrm{CS,equi}}$ = 14.6 nm is in very good agreement with $R_{\mathrm{CS,hom}}$ = 14 nm from the model-dependent form-factor analysis.

C. Dynamic light scattering (DLS)

1. Model-independent analysis

A CONTIN analysis of the experimentally obtained correlation functions reveals only one significant mode for all investigated concentrations of PB_{125}-PEO_{155} in water (0.02–0.2 wt. %). As an example $\bar{\Gamma}$ resulting from this mode is plotted against q^2 in Fig. 6 for the 0.2 wt. % solution. This gives a fairly good linear relationship over the entire q^2

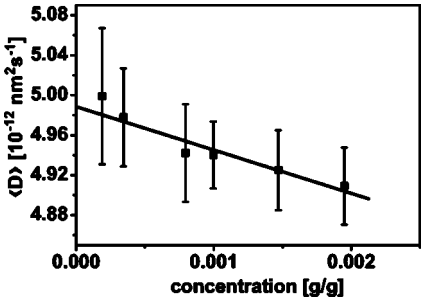

FIG. 7. The average apparent translational diffusion coefficient $\langle D_{z,\mathrm{app}}\rangle$ as a function of concentration c for solutions of PB_{125}-PEO_{155} in H_2O. The straight line indicates a linear fit.

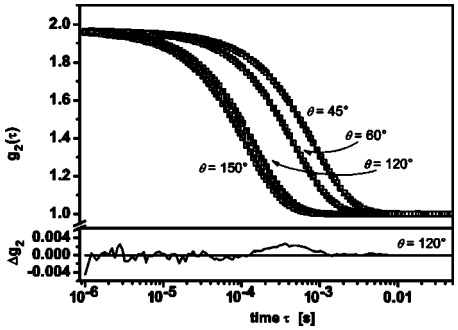

FIG. 8. Experimental intensity autocorrelation functions $g_2(\tau)$ at four scattering angles θ of a 0.2 wt. % solution of PB_{125}-PEO_{155} in H_2O with the respective simultaneous fit using the Pecoramodel for rigid rods with polydisperse length (lines). The quality of the fit is indicated by $\Delta g_2 = g_2(\tau)_{\mathrm{fit}} - g_2(\tau)_{\mathrm{measur.}}$ at $\theta = 120°$ as an example.

range, where the slope can be identified as the averaged apparent translational diffusion coefficient $\langle D_{z,\mathrm{app}}\rangle$ of the polymer aggregates. In this case "averaged" means that $\langle D_{z,\mathrm{app}}\rangle$ is derived from the whole experimental q range. However, at low-q values a deviation from the linear relation is observable and the intercept of the linear fit is significantly below zero. This is an indication for additional contributions to the dynamic behavior in addition to the pure translational motion. Therefore, the data are analyzed applying the model of Pecora for stiff rods (see below), which takes into account the rotational diffusion. The influence of internal dynamics and rotation decreases with decreasing q. Therefore, a linear regression of the two Γ values at the two lowest q values is performed, too (see Fig. 6). This gives low-q values of $D_{z,\mathrm{app}}$, which might represent the pure translational motion. But the errors are high (10%) due to the bad statistics by using only two data points for the regression. The found intercepts are in the range of 0 to −60 and no systematic dependence on the concentration c is observed for both the slope and the intercept. The mean value of $D_{z,\mathrm{app}}$ is $\overline{D_{z,\mathrm{app}}} = 4 \pm 0.4 \times 10^{-2}\ \mathrm{nm^2\ s^{-1}}$, which gives a value for the hydrodynamic radius $R_{H,z} = 60 \pm 6$ nm. The estimated error of $\overline{D_{z,\mathrm{app}}}$ covers all observed values of $D_{z,\mathrm{app}}$. Nevertheless, $\langle D_{z,\mathrm{app}}\rangle$ from the linear regressions over the whole q range as a function of concentration c is shown in Fig. 7 to investigate the concentration dependence of D_z. $\langle D_{z,\mathrm{app}}\rangle$ as a function of concentration has a slightly negative slope, which might be an indication that there are some attractive interactions between the aggregates or that the length of the aggregates increases slightly with increasing concentration.

2. Model-dependent analysis

In Fig. 8 the experimental intensity time correlation functions $g_2(\tau)$ for a 0.2 wt. % solution of PB_{125}-PEO_{155} at four different angles $\theta = 45°$, 60°, 120°, and 150° are shown. Under the justified assumption (see static light scattering) that the investigated aggregates have the shape of a rod, are markedly stiff and show a length distribution, it is possible to calculate theoretical correlation functions according to the model by Pecora with a Schulz-Zimm distributed length L. To increase the precision of the computed adjustable parameters, a simultaneous fit of $g_2(\tau)$ at four scattering angles according to Eq. (19) is performed. The angular dependence of the computed theoretical correlation functions is in good agreement with the experimental angular dependence. As an example the residuals for $\theta = 120°$ are depicted in Fig. 8. Only some minor deviations at large times are observed and the model represents the measured data with good accuracy. These minor deviations can be attributed to an imperfect representation of the length distribution by the Schulz-Zimm relation. During the fitting procedure the diameter d is fixed to a constant value. Varying the diameter d gives different values for the length L, and so different pairs of diameter and length can describe the experimental curves. The χ^2 values of the fits were plotted as a function of the diameter d, and this curve showed a minimum for a diameter of 26–30 nm for the investigated solutions ($c = 0.02$–0.2 wt. %). The corresponding mass averaged length is $L_w = 340$ nm and the found values for the polydispersity M_w/M_n are in the range of 1.5–2. The accuracy of these parameters does not allow for an analysis of the concentration dependence, since the concentration dependence is small.

V. CONCLUSION

In the present article the characterization of PB_{125}-PEO_{155} aggregates in aqueous solution is discussed. The shown experiments cover the concentration range from 0.02 wt. % up to 2 wt. %. The static light scattering data from a 0.02 wt.% solution can be described with a model form factor for rods and wormlike chains with a Schulz-Zimm distribution of the length L. The fit for the wormlike chain results in a ratio $L_w/L_K \approx 1$, i.e., a low flexibility of the rodlike aggregates. The mass-average length L_w of the aggregates resulting from these model fits is 389 and 380 nm, respectively, and the polydispersity parameter $M_w/M_n = 1.2$ and 2. In both cases the determined values reproduce the radius of gyration $R_{g,z} = 124$ nm found by analyzing the initial slope of $Kc/R(q)$ vs q^2 with good accuracy. From the molar mass of the aggregates $M_w = (1.65 \pm 0.5) \times 10^8\ \mathrm{g\ mol^{-1}}$ and the molar mass of one PB_{125}-PEO_{155} molecule $M_{w,p} = 13\,570\ \mathrm{g\ mol^{-1}}$ the aggregation number is calculated to be $N_{M_w} = 12100$.

Model-dependent analyses of the intensity-autocorrelation function $g_2(\tau)$ from the dynamical light scattering using the

model of Pecora for rigid rods, gives a mean length L_w of 340 ± 30 nm and a diameter of around 28 nm for solutions from 0.02 up to 0.2 wt. % concentration. The used model accounts for all relevant modes in the entire q range and for the present dimensions of length L. This is different compared to most of the previous DLS studies of rigid rod systems were usually only the first two modes are used to describe the decay of the correlation function. The decrease of $D_{z,\mathrm{app}}$ with inceasing polymer concentration is small. A growth of the length L of the aggregates with increasing polymer concentration would be directly observable in a concise decrease of $D_{z,\mathrm{app}}$ and we can conclude that the cylinder length is independent of the polymer concentration. This behavior is different compared to surfactant systems, which form wormlike micelles in aqueous solution. Such "living polymer" systems often show a concentration dependence according to a power law, viz. $L \propto c^{0.5}$ (e.g., $C_{12}E_5$ [40]).

The analysis of SANS data on 2 wt. % solution in D_2O shows a structure factor effect at low-q values. The maximum cross-sectional radius is $R_{\mathrm{CS,max}} = 19$ nm and the radial scattering length density profile $\sigma(r)$ is typical for a core-shell particle.

From the determined length L_w of the aggregates a linear particle density $N_{M_w,\mathrm{nm}} = 35\ \mathrm{nm}^{-1}$ is calculated. From the aggregate and polymer volume an aggregation number $N_V = 11\,240$ and a linear particle density $N_{V,\mathrm{nm}} = 32\ \mathrm{nm}^{-1}$ are calculated.

The found cylindrical aggregate shape and the dimensions of the cross section are in good agreement with the findings of Bates and co-workers. The number ratio $N_{\mathrm{PEO}}/N_{\mathrm{total}}$ of the present BCP is 0.55 and a cylindrical shape of the aggregates can be assumed. In contrast to other aqueous BCP solutions the present BCP forms only cylindrical aggregates and no coexistence with spherical aggregates or vesicles is observed.

ACKNOWLEDGMENTS

Financial support for this research from the Deutsche Forschungsgemeinschaft through SFB 448 is gratefully acknowledged.

[1] J. Seils and T. Dorfmüller, Biopolymers **31**, 813 (1991).
[2] S. Förster, Ber. Bunsenges. Phys. Chem. **101**, 1671 (1997).
[3] H.-P. Hentze, E. Krämer, B. Berton, S. Förster, M. Antonietti, and M. Dreja, Macromolecules **32**, 5803 (1999).
[4] A. C. Edrington, A. M. Urbas, P. DeRege, C. X. Chen, T. M. Swager, N. Hadjichristidis, M. Xenidou, L. J. Fetters, J. D. Joannopoulos, Y. Fink, and E. L. Thomas, Adv. Mater. (Weinheim, Ger.) **13**, 421 (2001).
[5] T. Liu, Z. Zhou, C. Wu, V. M. Nace, and B. Chu, Macromolecules **30**, 7624 (1997).
[6] T. Liu, V. M. Nace, and B. Chu, Langmuir **15**, 3109 (1999).
[7] G.-E. Yu, Z. Yang, M. Ameri, D. Attwood, J. H. Collett, C. Price, and C. Booth, J. Phys. Chem. B **101**, 4394 (1997).
[8] G.-E. Yu, H. Li, C. Price, and C. Booth, Langmuir **18**, 7756 (2002).
[9] V. Schädler, C. Nardin, U. Wiesner, and E. Mendes, J. Phys. Chem. B **104**, 5049 (2000).
[10] V. Bogomolov, S. V. Gaponenko, I. N. Germanenko, A. M. Kapitonov, E. P. Petrov, N. V. Gaponenko, A. V. Prokofiev, A. N. Ponyavina, N. I. Silvanovich, and S. M. Samoilovich, Phys. Rev. E **55**, 7619 (1997).
[11] D. C. Wang and A. P. Gast, J. Phys.: Condens. Matter **11**, 10133 (1999).
[12] H. Miguez, F. Meseguer, C. Lopez, F. Lopez-Tejeira, and J. Sanchez-Dehesa, Adv. Mater. (Weinheim, Ger.) **13**, 393 (2001).
[13] T. Palberg, J. Phys.: Condens. Matter **11**, R323 (1999).
[14] T. Hellweg, C. D. Dewhurst, E. Brückner, K. Kratz, and W. Eimer, Colloid Polym. Sci. **278**, 972 (2000).
[15] J. Bibette, J. Colloid Interface Sci. **147**, 474 (1991).
[16] H. Schlaad, H. Kukula, J. Rudloff, and I. Below, Macromolecules **34**, 4302 (2001).
[17] H. Schlaad, T. Krasia, and C. S. Patrickios, Macromolecules **34**, 7585 (2001).
[18] A. Kelarakis, V. Havredaki, G.-E. Yu, L. Derici, and C. Booth, Macromolecules **31**, 944 (1998).
[19] K. Nakashima, T. Anzai, and Y. Fujimoto, Langmuir **10**, 658 (1994).
[20] M. Wilhelm, C.-L. Zhao, Y. Wang, R. Xu, M. A. Winnik, J.-L. Mura, G. Riess, and M. D. Croucher, Macromolecules **24**, 1033 (1991).
[21] C. V. Nicholas, Y.-Z. Luo, N.-J. Deng, D. Attwood, J. H. Collett, C. Price, and C. Booth, Polymer **34**, 138 (1993).
[22] G. Wanka, H. Hoffmann, and W. Ulbricht, Macromolecules **27**, 4145 (1994).
[23] M. Y. Kozlov, N. S. Melik-Nubaroy, E. V. Batrakova, and A. V. Kabanov, Macromolecules **33**, 3305 (2000).
[24] Y. Zheng, Y.-Y. Won, F. S. Bates, H. T. Davis, L. E. Scriven, and Y. Talmon, J. Phys. Chem. B **103**, 10 331 (1999).
[25] Y.-Y. Won, A. Brannan, H. T. Davis, and F. S. Bates, J. Phys. Chem. B **106**, 3354 (2002).
[26] Y.-Y. Won, H. T. Davis, F. S. Bates, M. Agamalian, and G. D. Wignall, J. Phys. Chem. B **104**, 7134 (2000).
[27] S. Förster, B. Berton, H.-P. Hentze, E. Krämer, M. Antonietti, and P. Lindner, Macromolecules **34**, 4610 (2001).
[28] S. Förster and E. Krämer, Macromolecules **32**, 2783 (1999).
[29] P. S. Russo, *Dynamic Light Scattering From Rigid and Nearly Rigid Rods*, 1st ed. (Clarendon Press, Oxford, 1993), Chap. 12.
[30] B. J. Berne and R. Pecora, *Dynamic Light Scattering* (Wiley, New York, 1976).
[31] R. Pecora, J. Chem. Phys. **49**, 1036 (1968).
[32] T. M. Bender, R. J. Lewis, and R. Pecora, Macromolecules **19**, 244 (1986).
[33] P. Hiemenz, *Principles of Colloid and Surface Chemistry* (Marcel Dekker, New York, 1977).
[34] W. Burchard, Makromol. Chem., Macromol. Symp. **18**, 1 (1988).
[35] G. C. Berry, J. Chem. Phys. **44**, 4550 (1966).

[36] J. S. Pedersen, Adv. Colloid Interface Sci. **70**, 171 (1997).
[37] J. Drögemeier, H. Hinssen, and W. Eimer, Macromolecules **27**, 87 (1994).
[38] P. Lang, J. K. Kajiwara, and W. Burchard, Macromolecules **26**, 3992 (1993).
[39] T. Fuetterer, T. Hellweg, G. H. Findenegg, J. Frahn, and A. D. Schlüter (unpublished).
[40] U. Menge, P. Lang, and G. Findenegg, Colloids Surf., A **163**, 81 (2000).
[41] M. Schmidt and W. H. Stockmayer, Macromolecules **17**, 509 (1984).
[42] R. Koyama, J. Phys. Soc. Jpn. **34**, 1029 (1973).
[43] D. Potschke, P. Hickl, M. Ballauff, P. O. Astrand, and J. S. Pedersen, Macromol. Theory Simul. **9**, 345 (2000).
[44] J. S. Pedersen and P. Schurtenberger, Macromolecules **29**, 7602 (1996).
[45] M. Gradzielski, D. Langevin, and B. Farago, Phys. Rev. E **53**, 3900 (1996).
[46] T. Hellweg and D. Langevin, Physica A **264**, 370 (1999).
[47] I. W. Hamley, J. S. Pedersen, C. Booth, and V. M. Nace, Langmuir **17**, 6386 (2001).
[48] C. Graf, M. Deggelmann, M. Hagenbüchle, H. Kramer, R. Krause, C. Martin, and R. Weber, J. Chem. Phys. **95**, 6284 (1991).
[49] J. Schneider, D. Karrer, J. K. G. Dhont, and R. Klein, J. Chem. Phys. **87**, 3008 (1987).
[50] O. Glatter, Acta Phys. Austriaca **47**, 83 (1977).
[51] O. Glatter, J. Appl. Crystallogr. **13**, 7 (1980).
[52] O. Glatter, R. Strey, K.-V. Schubert, and E. W. Kaler, Ber. Bunsenges. Phys. Chem. **100**, 323 (1996).
[53] O. Glatter and O. Kratky, *Small Angle X-ray Scattering* (Academic Press, London, 1982).
[54] R. Zwanzig, Annu. Rev. Phys. Chem. **16**, 67 (1965).
[55] S. W. Provencher, Comput. Phys. Commun. **27**, 213 (1982).
[56] S. W. Provencher, Comput. Phys. Commun. **27**, 229 (1982).
[57] M. Doi and S. F. Edwards, *The Theory of Polymer Dynamics* (Clarendon Press, Oxford, UK, 1986).
[58] S. Broersma, J. Chem. Phys. **32**, 1626 (1960).
[59] S. Broersma, J. Chem. Phys. **32**, 1632 (1960).
[60] C. Tanford, J. Phys. Chem. **76**, 3020 (1972).
[61] A. Nordskog, H. Egger, G. H. Findenegg, T. Hellweg, H. Schlaad, H. v. Berlepsch, and C. Boettcher, Phys. Rev. E **68**, 011406 (2003).
[62] A. Nordskog, T. Fuetterer, G. H. Findenegg, T. Hellweg, H. v. Berlepsch, C. Boettcher, A. Heinemann, and H. Schlaad, Phys. Chem. Chem. Phys. **6**, 3123 (2004).
[63] U. Menge, P. Lang, G. H. Findenegg, and P. Strunz, J. Phys. Chem. B **107**, 1316 (2003).
[64] J. S. Pedersen, D. Posselt, and K. Mortensen, J. Appl. Crystallogr. **23**, 321 (1990).
[65] P. Hickl, M. Ballauff, and A. Jada, Macromolecules **29**, 4006 (1996).